

Blended-NeRF: Zero-Shot Object Generation and Blending in Existing Neural Radiance Fields

ORI GORDON, The Hebrew University of Jerusalem, Israel
 OMRI AVRAHAMI, The Hebrew University of Jerusalem, Israel
 DANI LISCHINSKI, The Hebrew University of Jerusalem, Israel

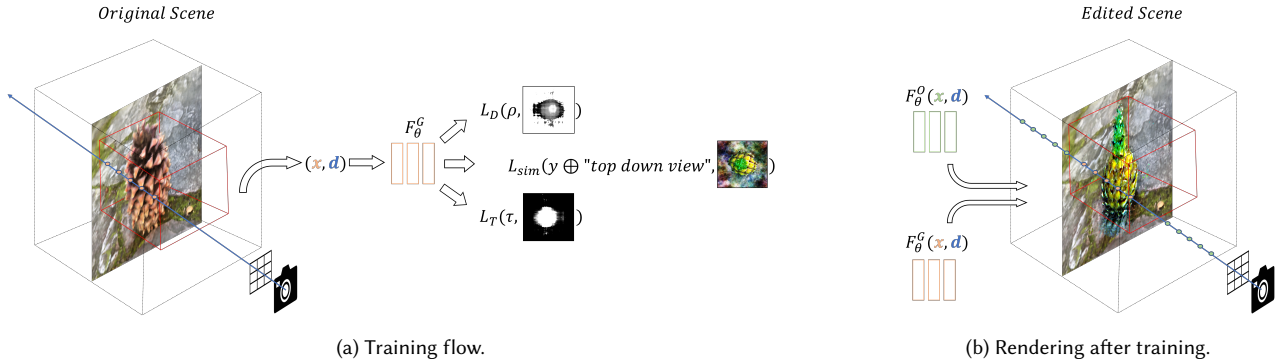


Fig. 1. Overview of the training and blending process. (a) Given a NeRF scene F_θ^O , our pipeline trains a NeRF generator model F_θ^G , guided by a similarity loss defined by a language-image model such as CLIP [Radford et al. 2021], to synthesize a new object inside a user-specified ROI. This is achieved by casting rays and sampling points for the rendering process [Mildenhall et al. 2020] only inside the ROI box. Our method introduces augmentations and priors to get more natural results. (b) After training, we render the edited scene by blending the sample points generated by the two models along each view ray.

Editing a local region or a specific object in a 3D scene represented by a NeRF is challenging, mainly due to the implicit nature of the scene representation. Consistently blending a new realistic object into the scene adds an additional level of difficulty. We present Blended-NeRF, a robust and flexible framework for editing a specific region of interest in an existing NeRF scene, based on text prompts or image patches, along with a 3D ROI box. Our method leverages a pretrained language-image model to steer the synthesis towards a user-provided text prompt or image patch, along with a 3D MLP model initialized on an existing NeRF scene to generate the object and blend it into a specified region in the original scene. We allow local editing by localizing a 3D ROI box in the input scene, and seamlessly blend the content synthesized inside the ROI with the existing scene using a novel volumetric blending technique. To obtain natural looking and view-consistent results, we leverage existing and new geometric priors and 3D augmentations for improving the visual fidelity of the final result.

We test our framework both qualitatively and quantitatively on a variety of real 3D scenes and text prompts, demonstrating realistic multi-view consistent results with much flexibility and diversity compared to the baselines. Finally, we show the applicability of our framework for several 3D editing applications, including adding new objects to a scene, removing/replacing/altering existing objects, and texture conversion.

Project page is available at <https://www.vision.huji.ac.il/blended-nerf/>.

1 INTRODUCTION

In the last few years we have witnessed exciting developments in neural implicit representations [Dupont et al. 2021; Liu et al. 2022; Sitzmann et al. 2020b; Strümpler et al. 2022; Su et al. 2022;

Authors' addresses: Ori Gordon, The Hebrew University of Jerusalem, Jerusalem, Israel, ori.gordon@mail.huji.ac.il; Omri Avrahami, The Hebrew University of Jerusalem, Jerusalem, Israel, omri.avrahami@mail.huji.ac.il; Dani Lischinski, The Hebrew University of Jerusalem, Jerusalem, Israel, danix@mail.huji.ac.il.

Szatkowski et al. 2022]. In particular, implicit representations of 3D scenes [Barron et al. 2021, 2022; Jiang et al. 2020; Mescheder et al. 2019; Mildenhall et al. 2020; Park et al. 2019; Sitzmann et al. 2020a, 2019] have enabled unprecedented quality and reliability in 3D reconstruction and novel view synthesis. The pioneering work of Mildenhall et al. [2020] introduced NeRFs, MLP-based neural models that implicitly represent a scene as a continuous volume and radiance fields from a limited number of observations, producing high-quality images from novel views via volume rendering.

However, editing a scene represented by a NeRF is non-trivial, mainly because the scene is encoded in an implicit manner by the model's weights, in contrast to explicit representations, such as meshes, voxel grids, or point clouds. NeRFs offer no explicit separation between the various components that define the object, such as shape, color, or material. Blending a new object into a NeRF-represented scene is even more challenging due to the requirement for consistency across multiple views between the new and the original NeRF scenes, as it requires multi-view information on top of the implicit representation challenges. This is in contrast to local edits in images, e.g., [Avrahami et al. 2022a,b; Bau et al. 2021; Brooks et al. 2022; Ho et al. 2020a; Nichol et al. 2021; Ramesh et al. 2022], where the blending is done in pixel space with all the required information appearing in a single view.

The first works attempting to edit NeRF scenes focused on the removal of local parts, changing color, or shape transfer on one class of synthetic data, guided by user scribbles or latent code of another object in the class [Liu et al. 2021]. In CLIP-NeRF [Wang et al. 2022a], editing of the entire scene is performed by text or image guidance and displacements to the latent representation of the input. They

mainly focus on synthetic objects from one class, or global color changes for realistic scenes. Kobayashi et al. [2022] perform semantic decomposition of the scene components by learning a feature field that maps each 3D coordinate to a descriptor representing a semantic feature, and allow zero-shot segmentation for local editing on a specific semantic class. Alternatively, Benaim et al. [2022] suggest separating the volumetric representation of a foreground object from its background using a set of 2D masks per training view. These works have limited localization abilities and focus on the separation methods. They demonstrate simple manipulations such as object removal, color change, and transformations such as shift, rotation, and scale.

In this work, we present our approach for ROI-based editing of NeRF scenes guided by a text prompt or an image patch that: (1) can operate on any region of a real-world scene, (2) modifies only the region of interest, while preserving the rest of the scene without learning a new feature space or requiring a set of two-dimensional masks, (3) generates natural-looking and view-consistent results that blend seamlessly with the existing scene, (4) is not restricted to a specific class or domain, and (5) enables complex text guided manipulations such as object insertion/replacement, objects blending and texture conversion.

To this end, we utilize a pretrained language-image model, e.g., CLIP [Radford et al. 2021], and a NeRF model [Mildenhall et al. 2020] initialized on existing NeRF scene as our generator for synthesizing a new object and blend it into the scene in the region of interest (ROI). We use CLIP to steer the generation process towards the user-provided text prompt or an image patch, enabling blended generation of diverse 3D objects.

To enable general local edits in any region, while preserving the rest of the scene, we first present the user with a simple GUI for localizing a 3D box inside a given NeRF scene, leveraging depth information from the NeRF for intuitive feedback. For seamless blending of the synthesized content inside the ROI with the base scene, we propose a novel volumetric blending approach that merges the original and the synthesized radiance fields by blending the sampled 3D points along each camera ray.

We show that using this pipeline naively to perform the edit is insufficient, generating low quality incoherent and inconsistent results. Thus, we utilize the augmentations and priors suggested in [Jain et al. 2022] and introduce additional priors and augmentations, such as depth regularization, pose sampling, and directional dependent prompts to get more realistic, natural-looking and 3D consistent results. Finally, we conduct extensive experiments to evaluate our framework and the effect of our additional constraints and priors. We perform an in-depth comparison with the baseline and show the applicability of our approach on a series of 3D editing applications using a variety of real 3D scenes.

2 RELATED WORK

Neural Implicit Representations have gained much popularity in the fields of computer vision and graphics in both 2D and 3D [Dupont et al. 2021; Jiang et al. 2020; Mescheder et al. 2019; Park et al. 2019; Sitzmann et al. 2020a,b, 2019; Strümpler et al. 2022]. Among

their advantages is their ability to capture complex and diverse patterns and to provide a continuous representation of the underlying scene. They are resolution independent, yet compact, compared to explicit representations of high resolution 2D images, or meshes and point clouds in 3D. NeRFs [Barron et al. 2021, 2022; Mildenhall et al. 2020] learn to represent a 3D scene as a continuous volume and radiance fields using the weights of a multilayer perceptron (MLP). Given a 3D position x and view direction (θ, ϕ) , NeRF outputs the density σ and color c at x . Novel views of the scene can thus be rendered by accumulating the colors and densities along a view ray $\mathbf{r}(t)$ passing through each pixel, using an approximation to the classical volume rendering equation using the quadrature rule [Max 1995]:

$$C(\mathbf{r}) = \sum_{i=1}^N T_i (1 - \exp(-\sigma_i \delta_i)) c_i, \quad T_i = \exp\left(-\sum_{j=1}^{i-1} \sigma_j \delta_j\right), \quad (1)$$

where $\delta_i = t_{i+1} - t_i$ is the distance between adjacent samples and T_i can be interpreted as the degree of transmittance at point x_i along the ray. The inputs are embedded into a high-dimensional space using a high frequency sinusoidal positional encoding $\gamma(x)$ to enable better fitting for high frequency variations in the data [Rahaman et al. 2019; Tancik et al. 2020]:

$$\gamma(x) = [\cos(2^l x), \sin(2^l x)]_{l=0}^{L-1} \quad (2)$$

NeRF 3D Generation. NeRFs inspired follow-up works to synthesize new NeRF objects from scratch. The first methods used NeRF combined with GANs [Arjovsky et al. 2017; Goodfellow et al. 2014; Gulrajani et al. 2017] to design 3D-aware generators [Chan et al. 2021; DeVries et al. 2021; Gu et al. 2022; Niemeyer and Geiger 2021a,b; Schwarz et al. 2020; Zhou et al. 2021]. GRAF [Schwarz et al. 2020] adopts shape and appearance codes to conditionally synthesize NeRF and GIRAFF [Niemeyer and Geiger 2021b], StyleNeRF [Gu et al. 2022] utilizes NeRF to render features instead of RGB colors and adopt a two-stage strategy, where they render low-resolution feature maps first and then up-sample the feature maps using a CNN decoder. These models are category-specific and trained mostly on forward-facing scenes.

More recent works utilize the progress in contrastive representation learning [Desai and Johnson 2021; Li et al. 2023, 2022a; Radford et al. 2021; Zhai et al. 2022], which enables easy and flexible control over the content of the generated objects using textual input. In Dream Fields [Jain et al. 2022], frozen image-text joint embedding models from CLIP [Radford et al. 2021] are used as a guidance to a NeRF model that generates 3D objects whose renderings have high semantic similarity with the input caption. To improve the visual quality, they introduce simple geometric priors and augmentations to enforce transmittance sparsity, object boundaries and multi-view consistency. In this paper, we utilize some of the priors from Dream Fields [Jain et al. 2022] and introduce improved augmentations and priors to edit existing NeRF scenes.

More recent works utilize the progress in diffusion models [Ho et al. 2020b; Song et al. 2021; Song and Ermon 2020] and specifically in text-conditioned diffusion models [Ramesh et al. 2022; Rombach et al. 2022; Saharia et al. 2022]. DreamFusion [Poole et al. 2023] and its follow-ups [Lin et al. 2023; Metzer et al. 2022; Wang et al. 2022b]

optimize a NeRF model by replacing CLIP with score function losses using pretrained text-conditioned 2D diffusion-models applied on many different views of the generated scene to synthesize 3D objects aligned with the input text. These models synthesize new objects without considering how they can be inserted and blend into an existing scene.

Editing NeRFs. The pioneering works [Liu et al. 2021; Wang et al. 2022a] were the first to tackle the challenge of editing NeRF scenes. They both define a conditional NeRF, where the NeRF model is conditioned on latent shape and appearance codes, which enables separately editing the shape and the color of a 3D object. EditNeRF [Liu et al. 2021] only enables addition and removal of local parts or color changes guided by user scribbles and is limited to only one shape category. CLIP-NeRF [Wang et al. 2022a] leverage the joint language-image embedding space of CLIP [Radford et al. 2021] to perform text or image guided manipulation on the entire scene. During the optimization it uses two code mappers for the shape and appearance that receive the CLIP embedding and output shape and appearance codes which steer the input of the model and the model weights to apply the edit. The manipulation capabilities are demonstrated mainly on synthetic objects from one class and on global color changes for realistic scenes.

Later works focused on geometric edits [Yuan et al. 2022], global style transfer [Chen et al. 2022; Chiang et al. 2022; Fan et al. 2022; Huang et al. 2022], recoloring [Gong et al. 2023; Wu et al. 2022], and disentanglement of the scene to enable local edits [Benaim et al. 2022; Kobayashi et al. 2022]. Kobayashi et al. [2022] decomposes the scene to its semantic parts by training the NeRF model to learn a 3D feature field using supervision of pre-trained 2D image feature extractors [Caron et al. 2021; Li et al. 2022b] in addition to learning of the volume density and the radiance field. After training, the model can perform zero-shot segmentation for local editing of a specific semantic class. Benaim et al. [2022] disentangle the volumetric representation of a foreground object from its background using a set of 2D masks specifying the foreground object in each training view. They train two models for the full scene and the background scene, and subtract the background from the full scene in order to get the foreground. In both works the localization on the region of interest is incomplete and not flexible enough (does not enable editing parts of objects, empty regions or blending new densities into the area of existing object). The demonstrated manipulations are simple ones, such as object removal, transformations such as shift rotation and scale, and only basic optimization-based edits. Our work focuses on blending text or image generated objects with volume and color into any region of interest of an existing scene with more freedom and flexibility and without compromising on quality and visibility. For information regarding concurrent works, please refer to the supplement.

3 METHOD

Given an existing 3D scene x_o represented by a NeRF model F_θ^O , and a 3D region of interest (ROI), indicated by a box B localized inside the scene, our goal is to modify the scene inside the ROI, according to a user-provided text prompt or image patch. In other words, we aim to obtain a modified scene x_e , where $x_e \odot B$ is consistent with

the user prompt from any point of view, while matching x_o outside the box ($x_e \odot (1 - B) = x_o \odot (1 - B)$). Furthermore, x_e should appear seamless across the boundaries of B .

To perform the edits inside the ROI we initialize a 3D MLP model F_θ^G with the weights of the original scene model F_θ^O and steer the weights towards the given prompt using a pretrained language-image model, such as CLIP [Radford et al. 2021]. We enable local edits in any region of the scene x_o by introducing a simple GUI for localizing a 3D box inside the scene by rendering the original NeRF model F_θ^O from any view and using the output depth map of the model to obtain 3D understanding of the scene. Using the given ROI box we can disentangle the scene inside the box and outside it by decomposing the radiance fields accordingly. To obtain seamlessly blended results from any view direction, we perform volumetric blending of the original and the edited radiance fields by sampling 3D points along each camera ray r in both F_θ^O and F_θ^G , and blending the samples while accounting for their densities, colors and distance from the center of the scene.

To get more realistic and natural-looking results we present existing [Jain et al. 2022] and novel augmentations and priors such as transmittance and depth regularization, background augmentations, pose sampling and directional dependent prompts. An overview of our approach is depicted in Figure 1a.

In Section 3.1 we describe our 3D object generation and blending process. We continue and present the model objectives and proposed priors in Section 3.2 and introduce our graphic interface for placing a 3D box in a desired location inside the scene in Section 3.3.

3.1 Image-Text driven 3D synthesis and blending

Given a 3D scene represented by a NeRF model F_θ^O , an ROI box B , and a camera pose, we use a duplicate of F_θ^O, F_θ^G as our starting point for generating the content of B . The rest of the scene is preserved by rendering only the rays which have sample points inside B . The training of F_θ^G is guided by a language-image model, e.g., [Li et al. 2023, 2022a; Radford et al. 2021; Zhai et al. 2022] to align the content generated inside B with a user-provided text prompt or image patch.

To get a smoothly blended result, we query both models F_θ^O, F_θ^G using the same set of rays. For sample points outside the ROI, we use the density and color inferred by F_θ^O , while for points inside the ROI, we blend the results of the two radiance fields using one of two modes, depending on the type of the edit: adding a new object in empty space, or completely replacing an existing one, vs. adding an object in a non-empty area.

F_θ^G is optimized using guidance from a language-image model, such as CLIP [Radford et al. 2021], by aiming to minimize the cosine similarity score between the user-provided text prompt y and rendered views of the generated content inside the ROI box, I_{ROI} :

$$L_{sim} = -E_{img}(I_{ROI})^T E_{txt}(y), \quad (3)$$

where E_{img}, E_{txt} are the image and text encoders of the image-language model (if the user guidance y is an image, $E_{img}(y)$ is used in place of $E_{txt}(y)$). During optimization, we render I_{ROI} using only the 3D sample points contained inside B by sampling only along rays r that pass through the box and setting the density to zero for

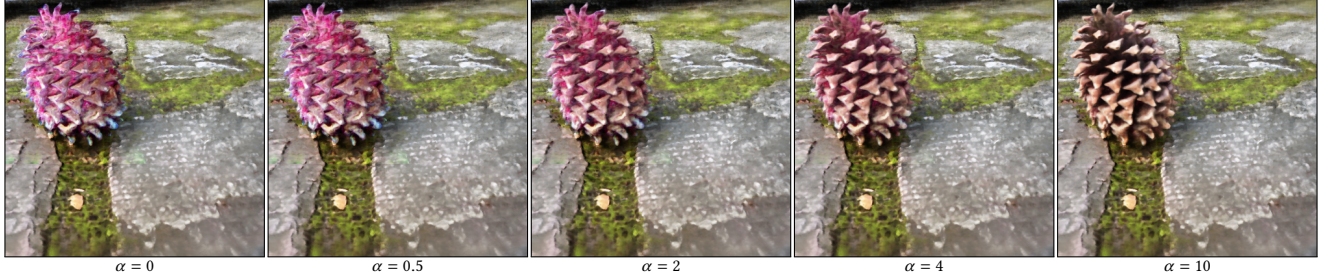


Fig. 2. **Distance Smoothing Operator.** We demonstrate our suggested smoothing operator in eq. (5) on a range of α values. When α is 0 all the weight goes to the edited scene, and as we increase α , more attention is given to closer points from the original scene.

all sample points outside B , according to eq. (1):

$$C(\mathbf{r}) = \begin{cases} \sum_{x_i \in B} T_i (1 - \exp(-\sigma_i \delta_i)) c_i, & \exists x_i \in \mathbf{r} \text{ s.t. } x_i \in B \\ 0, & \text{otherwise} \end{cases} \quad (4)$$

After training, we blend the scenes inside and outside the ROI with the same set of rays by querying both F_θ^O and F_θ^G where the points inside the box are rendered by F_θ^G and the points outside the box are rendered by F_θ^O . To get smooth blending between the two scenes we suggest distance smoothing operator per point inside the box considering its distance from the center of the ROI scene (center of mass, computed during training) and alpha compositing the density and color of the two scenes inside the ROI as follows:

$$f(\mathbf{x}) = 1 - \exp\left(\frac{-\alpha d(\mathbf{x})}{\text{diag}}\right) \quad (5)$$

$$\begin{aligned} \sigma_{\text{blend}}(\mathbf{x}) &= f(\mathbf{x}) \cdot \sigma_O(\mathbf{x}) + (1 - f(\mathbf{x})) \cdot \sigma_G(\mathbf{x}) \\ c_{\text{blend}}(\mathbf{x}) &= f(\mathbf{x}) \cdot c_O(\mathbf{x}) + (1 - f(\mathbf{x})) \cdot c_G(\mathbf{x}), \end{aligned}$$

where $d(\mathbf{x})$ is the Euclidean distance of a point \mathbf{x} inside the ROI from the center of the scene, diag is the box diagonal and α is a hyperparameter which controls the strength of the blending, as can be seen intuitively in Figure 2. The resulted raw densities and RGB values inside and outside the ROI are then blended along each ray using eq. (1) to get the current rendered view of the edited scene x_e .

Object Insertion/Replacement. In this mode, a new synthetic object is added into an empty region of the scene, or entirely replaces another existing object inside the ROI. In this mode, we use the pipeline described above, when inside the ROI we consider only the radiance field of F_θ^G during training. After training, we blend the two scenes as described above.

Object Blending. In contrast to the above mode, here we aim to blend the new content with the existing scene inside the ROI. We query both the original F_θ^O and the edited F_θ^G fields inside the box and blend the resulting colors and densities at each ray sample. To blend the sample colors, we first compute the alpha values for each point x_i on the ray separately from each model:

$$\begin{aligned} \alpha_O(x_i) &= 1 - \exp(\phi(\sigma_O(x_i)) \cdot \delta_i) \\ \alpha_G(x_i) &= 1 - \exp(\phi(\sigma_G(x_i)) \cdot \delta_i), \end{aligned} \quad (6)$$

where σ_O and σ_G are the densities returned by each model, and ϕ is the activation function enforcing that these density values are non-negative. To blend the colors c_O and c_G obtained from the

two models, we use the above alpha values, followed by a sigmoid function:

$$c(x_i) = \frac{c_O(x_i) \cdot \alpha_O(x_i) + c_G(x_i) \cdot \alpha_G(x_i)}{\epsilon + \alpha_O(x_i) + \alpha_G(x_i)}, \quad (7)$$

where ϵ is a small constant, for numerical stability.

For the density of the blended sample, we consider two options, which have different impact on the results of the blending:

$$\sigma(x_i) = \phi(\sigma_O(x_i) + \sigma_G(x_i)) \quad (8)$$

$$\sigma(x_i) = \phi(\sigma_O(x_i)) + \phi(\sigma_G(x_i))) \quad (9)$$

i.e., summing the densities inside or outside the activation function. When using eq. (8) we are summing inside the activation function thus allowing the generator F_θ^G to change the original scene density and even remove densities (if $\sigma_G(x_i) < 0$), while in eq. (9) we allow F_θ^G to only add new densities to the scene. We can choose either of these two options depending on the edit we wish to apply. We then compute the joint transmittance and alpha values according to eq. (1). The resulting blended image I_{ROI} is then used to guide F_θ^G during training by measuring its similarity to the input caption/image patch using eq. (3). The blending process after training is the same as in Object Insertion/Replacement mode. An illustration of our blending modes on the blender Lego scene is presented in Figure 3.

3.2 Objectives and Priors

Previous works [Benaim et al. 2022; Jain et al. 2022; Wang et al. 2022a] and our experiments indicate that a scene representation depending on similarity loss alone (eq. (3)) is too unconstrained, resulting in a scene that is not visually compatible to a human, but still satisfies the loss. Thus, we utilize the priors and augmentations mentioned in DreamFields [Jain et al. 2022] and suggest additional priors to get more realistic results.

Pose Sampling. CLIP-NeRF [Wang et al. 2022a] shows the multi-view consistency evaluation of CLIP [Radford et al. 2021]. When using different camera poses and rendering different views of the same object, they still have high similarity, in contrast to different objects which have low similarity even in identical view. DreamFields [Jain et al. 2022] shows that sampling different camera poses is a good regularizer and improves the realism of the object geometry. Thus, each iteration we sample a random camera pose around the scene depending on the scene type (360° and forward-facing scenes) including its azimuth and elevation angles (θ, ϕ) . We found

it is beneficial to be relatively close to the object during training to get a bigger object in the rendered view, which in turn yields larger gradients from eq. (3). We set the initial distance d from the ROI according to the camera $AFOV = 2\gamma$ and the maximum dimension of the box e_{max} and we randomly sample the radius r around this value:

$$d = \frac{e_{max}}{2 \tan(\gamma/2)} \quad (10)$$

Background Augmentation. DreamFields [Jain et al. 2022] note that when using white or black background during optimization, the scene populates the background, and eventually we get a diffused scene. Thus, we use the same random backgrounds as in DreamFields: Gaussian noise, checkerboard patterns and random Fourier textures from [Mordvintsev et al. 2018] to get more sharp and coherent objects.

Directional Dependent Prompts. Due to the fact that there's no constraint on F_θ^G to describe the object differently in different views, we concatenate to the original caption a text prompt depending on the current view. For more details, please refer to the supplementary materials.

Transmittance loss. Same as in DreamFields [Jain et al. 2022], in order to get more sparse and coherent results we encourage the generator to increase the average transmittance of the scene inside the box by adding a transmittance loss to the generator objective:

$$L_T = -\min(\tau, \text{mean}(T(P))) \quad (11)$$

When $\text{mean}(T(P))$ is the average transmittance of a rendered view from pose P and τ is the max transmittance.

Depth loss. When blending in forward-facing scenes (such as LLFF dataset [Mildenhall et al. 2019]) and due to the limited viewing intervals, for some captions we get a flat billboard geometry effect and the resulting edit does not seem to have a volume. We encourage the generator to synthesize volumetric 3D shapes by adding a depth

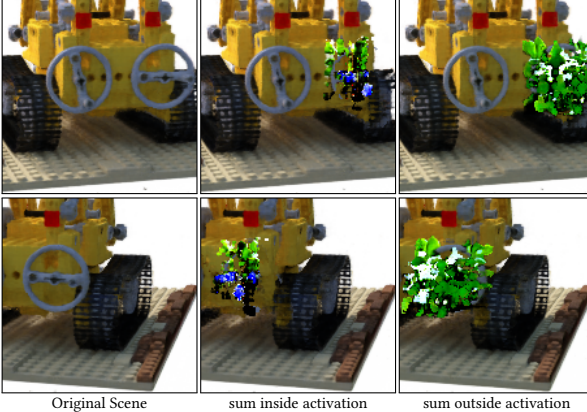


Fig. 3. **Blending Modes.** In the second column, when using eq. (8) we allow F_θ^G to change the density of the original scene, in this case removing parts of the wheel. When utilizing eq. (9) in the third column, we can only add additional density to the scene, so the plant warps around the wheel without changing it.

Table 1. **Quantitative Evaluation.** The proposed metrics evaluate the alignment of the edits to the text, the consistency between different views, and the background preservation. Our method archives edits that are better aligned to the input captions and consistent between views, while preserving the background of the scene.

Method	CLIP Direction Similarity ↑	CLIP Direction Consistency ↑	LPIPS ↓
[Benaim 2022]	0.128	0.736	0.3
ours	0.143	0.787	0.024

loss to the generator objective:

$$L_D = -\min(\rho, \sigma^2(D(P))) \quad (12)$$

When $\sigma^2(D(P))$ is the variance of the disparity map of a rendered view from pose P and ρ is the max variance we allow during training. We gradually introduce L_T and L_D during training using annealing strategy to prevent completely transparent or amorphous scenes. In summary, the final objective for the generator F_θ^G is:

$$L_{total} = L_{sim} + \lambda_T L_T + \lambda_D L_D \quad (13)$$

When λ_T, λ_D are the weights for L_T, L_D accordingly. For more information on implementation details and hyperparameters, please refer to the supplement.

3.3 ROI Specification Interface

To specify the ROI and use it to decompose the scene, we introduce a graphic interface that enables positioning an axis-aligned 3D box inside the scene. Given the 3D position of the center, as well as the axis dimensions, of the box, rendering of the scene is performed from the provided camera position using the original NeRF model F_θ^O . The edges of the 3D box are then projected onto the image plane using the camera matrix. To provide intuitive feedback regarding the location of the box in the scene, we utilize the depth map of the scene to remove parts of the box edges that are occluded by the scene. In this manner, the user is able to specify the ROI in a precise and intuitive way by moving the box and modifying its dimensions while being able to inspect the location from any point of view.

4 EXPERIMENTS

In Section 4.1 we begin by comparing our method both qualitatively and quantitatively to the baseline Volumetric Disentanglement for 3D Scene Manipulation [Benaim et al. 2022]. Next, in Section 4.2 we demonstrate the effect of our suggested priors and augmentations on improving fidelity and visual quality. Finally, in Section 4.3 we demonstrate several applications enabled by our framework.

4.1 Comparisons

Our qualitative comparisons to Volumetric Disentanglement [Benaim et al. 2022] are shown in Figure 4. Since the implementation of [Benaim et al. 2022] is not currently available, we perform the comparisons using the examples included on their project page¹. As can be seen from the results in Figure 4, our results exhibit richer and more natural colors and are aligned better with the text. To

¹<https://sagiebenaim.github.io/volumetric-disentanglement/>

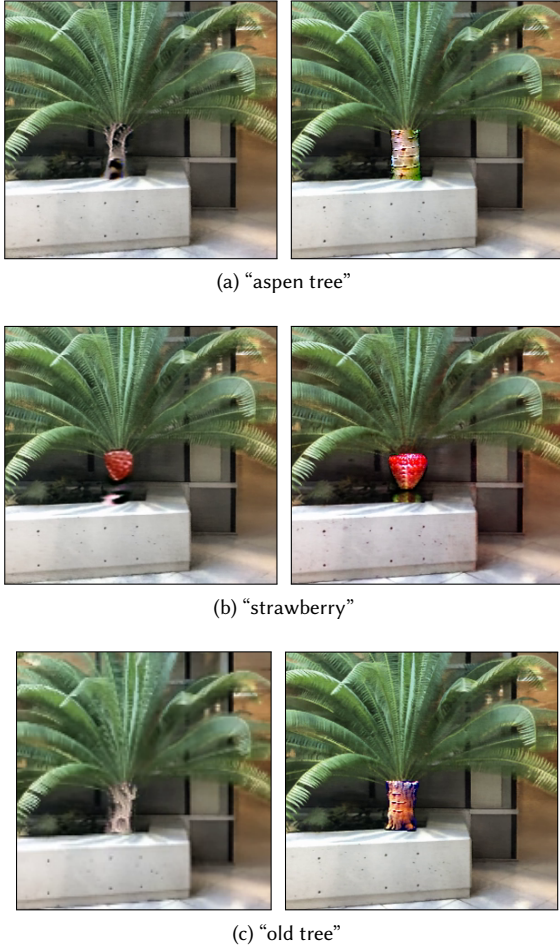


Fig. 4. Comparison to [Benaim et al. 2022] for object replacement. We compare our editing capabilities to [Benaim et al. 2022] in the fern scene from llff dataset [Mildenhall et al. 2019]. The left and right images in each row are [Benaim et al. 2022] and ours, accordingly. Each of the captions was concatenated to the prefix “a photo of a” before training, as recommended in [Radford et al. 2021]. Our proposed method exhibits more realistic results that agree better with the text. For example the edit for the text “aspen tree” indeed looks like a trunk of an aspen tree in our edit.

test these observations quantitatively, in Table 1 we compare our proposed method to [Benaim et al. 2022] using three metrics:

(1) CLIP Direction Similarity, a metric originally introduced in StyleGAN-NADA [Gal et al. 2021], measures how well the change between the original and edited views is aligned with the change in the texts describing them (in the CLIP embedding space).
(2) CLIP Direction Consistency, introduced by Haque et al. [2023], measures the cosine similarity of the CLIP embeddings of a pair of adjacent frames. For each edit, we take 6 consecutive frames, compute the metric for each consecutive pair, and average the results among all pairs.

Table 2. Ablation study. We test our proposed priors and augmentations on a subset of captions and images from COCO dataset [Lin et al. 2014]. The CLIP and BLIP R-Precision scores utilize CLIP B-32 and BLIP2 architecture accordingly. The first row shows the scores of the GT COCO image, the second row shows our method scores using all the priors and augmentations as described in Section 3 and the last two rows present the scores when taking out the directional dependent prompts and the depth loss.

Method	CLIP R-Precision \uparrow	BLIP R-Precision \uparrow
COCO GT images	0.933	0.98
Ours (full pipeline)	0.86	0.8
Ours (no dir prompts)	0.85	0.8
Ours (no depth prior)	0.81	0.78

Finally, we use (3) **LPIPS** [Zhang et al. 2018] to measure the difference between the original and edited scenes, with the ROI masked, for comparing the background preservation. As can be seen from Table 1, our model outperforms the baseline in all metrics, which implies that our generated objects match better to the input text captions, they are more consistent from any view and, on the other hand, our method manages to keep the rest of the scene untouched.

4.2 Ablation Study

To show the importance of our proposed augmentations and priors, we use the R-Precision score [Park et al. 2021] using both CLIP and BLIP [Li et al. 2023, 2022a; Radford et al. 2021] as the metric language-image model to measure how well the generated images align with the true caption. Similar to DreamFields [Jain et al. 2022], we use a randomly selected subset of 20 samples (due to time and resources limitations) from the object-centric dataset which contains 153 images and captions from COCO dataset [Lin et al. 2014] as our ground truth. The objects are synthesized using the given captions and blended into an empty region in the llff fern scene. Due to the fact we are training on the same CLIP model, we test our results with a different language-image model, BLIP2 [Li et al. 2023]. The results of both metrics are presented in Table 2. The directional dependent prompts seem to only slightly improve the results, probably due to the forward-facing nature of the scene. When rendering from limited camera positions and viewing angles and without our proposed depth priors, the results deteriorate. To test this conclusion visually, in Figure 5 we compare the task of inserting a new object into an empty region of the fern llff scene [Mildenhall et al. 2019] with and without the depth loss. As can be seen from the figure, when using our proposed depth prior, the generated object has more volume and looks more natural and consistent. For additional details, please refer to the supplement.

4.3 Applications

In this section, we demonstrate the applicability of our framework for several 3D editing scenarios.

New Object Insertion. Using the method described in Section 3, and by placing the ROI box in an empty space of the scene, we can synthesize a new object given a text prompt and blend it into the original scene. In Figure 6 we demonstrate such edits using several captions from COCO dataset [Lin et al. 2014].



Fig. 5. **Depth Loss Impact.** Comparison of synthesizing a “donut covered with glaze and sprinkles” from COCO dataset [Lin et al. 2014] on the limited view fern scene from llff dataset [Mildenhall et al. 2019] with and without our suggested depth prior. The first two columns display two views of the edited scenes, and the third column shows the object inside the ROI box. Finally, the last column displays the disparity map of the synthesized objects. In (a) the results are more flat, which can be clearly seen in the disparity map. Whereas in (b) we have a full 3D object which is more natural looking and consistent.

Object Replacement. To replace an existing object in the scene with new synthesized content, we place the ROI 3D box in the required area (enclosing the object to be replaced), and perform the training process described in Section 3. In Figure 7 we demonstrate the replacement of the sea in the blender ship scene, while in Figure 9 we replace the bottom part of the vase with flower petals.

Blending of Objects. To perform blending between the original and the generated object inside the ROI, we utilize the object blending process described in Section 3. In Figures 3 and 10 we demonstrate this blending on blender Lego and llff fern scenes.

Texture Editing. We enable texture editing by training only the color-related layers of F_θ^G and freezing all the other layers in a similar way as in [Wang et al. 2022a]. For seamless blending results, we utilize eq. (5). In Figure 8 we demonstrate this edit method on the pinecone 360 scenes. For additional results and videos please refer to supplement.

5 LIMITATIONS AND CONCLUSIONS

We introduced a novel solution to seamlessly blend new objects into an existing NeRF scene with natural looking and consistent results by utilizing a language-image model to steer the generation process towards the edit and by introducing novel priors, augmentations and volumetric blending techniques for improving the final edited scene. We tested our method on a variety of scenes and text prompts and showed the applicability of our framework on several editing applications. We believe that our framework can be utilized in a variety of applications due to the ease and intuitive interaction enabled by our interface.

One of the limitations of our framework is that currently it can’t edit multiple objects in a given scene, such as changing two wheels of a 3D car without impacting the rest of the scene. Additionally, the use of a box as our ROI scene shape can be sometimes limiting; for example, when trying to edit a circular scene like the blender ship scene in Figure 7, a cylinder could be preferable. Due to the fact we are rendering one view in each training step, we may get artifacts like multiple heads on the generated object. The quality of our generated objects can be improved by utilizing the recent progress in diffusion models, we leave it as a future work to combine our suggested blending framework with these models.



Fig. 6. **Object Insertion.** Insertion of new objects from COCO dataset [Lin et al. 2014] into an empty region in fern llff scene. Each column shows two views of the same edited scene [Mildenhall et al. 2019].



Fig. 7. **Large object replacement.** Here we perform object replacement to the blender ship scene by localizing the ROI box to include the sea and the bottom of the ship and training our model to steer the edit towards the given text prompts.

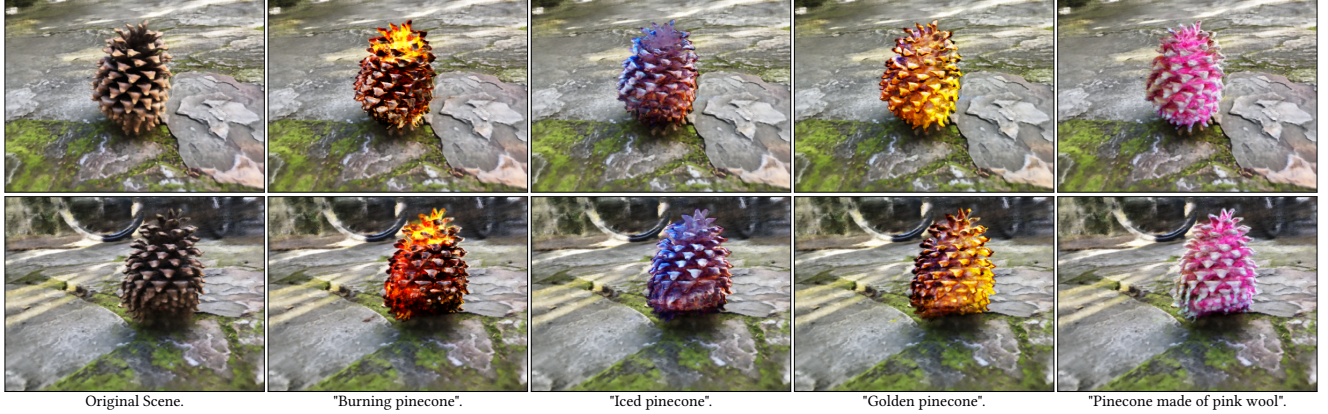


Fig. 8. **Texture Editing.** We can change only the texture of an object by freezing the layers responsible for the density and training only the layers that impact the color of the scene. To get a smooth blending, we utilize eq. (5) to blend the scene inside and outside the ROI.



Fig. 9. **Object Insertion in vasedeck 360 scene.** We used the text: "a photo of a purple, white and blue flowers petals on the ground" and eq. (5) with $\alpha = 3.5$ to generate the edit.



Fig. 10. **Blending Densities Inside Activation.** We demonstrate our suggested blending procedure for blending the original and synthesized objects inside the ROI in llff fern scene [Mildenhall et al. 2019] using eq. (8) for summing the densities.

REFERENCES

Martin Arjovsky, Soumith Chintala, and Léon Bottou. 2017. Wasserstein Generative Adversarial Networks. 70 (2017).

Omri Avrahami, Ohad Fried, and Dani Lischinski. 2022a. Blended Latent Diffusion. *ArXiv* abs/2206.02779 (2022).

Omri Avrahami, Dani Lischinski, and Ohad Fried. 2022b. Blended diffusion for text-driven editing of natural images. In *Proceedings of the IEEE/CVF Conference on Computer Vision and Pattern Recognition*. 18208–18218.

Chong Bao, Yinda Zhang, Bangbang Yang, Tianxing Fan, Zesong Yang, Hujun Bao, Guofeng Zhang, and Zhaopeng Cui. 2023. SINE: Semantic-driven Image-based NeRF Editing with Prior-guided Editing Field. *arXiv preprint arXiv:2303.13277* (2023).

Jonathan T Barron, Ben Mildenhall, Matthew Tancik, Peter Hedman, Ricardo Martin-Brualla, and Pratul P Srinivasan. 2021. Mip-nerf: A multiscale representation for anti-aliasing neural radiance fields. In *Proceedings of the IEEE/CVF International Conference on Computer Vision*. 5855–5864.

Jonathan T Barron, Ben Mildenhall, Dor Verbin, Pratul P Srinivasan, and Peter Hedman. 2022. Mip-nerf 360: Unbounded anti-aliased neural radiance fields. In *Proceedings of the IEEE/CVF Conference on Computer Vision and Pattern Recognition*. 5470–5479.

David Bau, Alex Andonian, Audrey Cui, YeonHwan Park, Ali Jahanian, Aude Oliva, and Antonio Torralba. 2021. Paint by word. *arXiv preprint arXiv:2103.10951* (2021).

Sagie Benaim, Frederik Warburg, Peter Ebert Christensen, and Serge Belongie. 2022. Volumetric Disentanglement for 3D Scene Manipulation. *ArXiv* abs/2206.02776 (2022).

Tim Brooks, Aleksander Holynski, and Alexei A Efros. 2022. Instructpix2pix: Learning to follow image editing instructions. *arXiv preprint arXiv:2211.09800* (2022).

Mathilde Caron, Hugo Touvron, Ishan Misra, Hervé Jégou, Julien Mairal, Piotr Bojanowski, and Armand Joulin. 2021. Emerging properties in self-supervised vision transformers. In *Proceedings of the IEEE/CVF international conference on computer vision*. 9650–9660.

Eric R. Chan, Marco Monteiro, Petr Kellnhofer, Jiajun Wu, and Gordon Wetzstein. 2021. Pi-GAN: Periodic Implicit Generative Adversarial Networks for 3D-Aware Image Synthesis. In *Proceedings of the IEEE/CVF Conference on Computer Vision and Pattern Recognition (CVPR)*. 5799–5809.

Yaosen Chen, Qi Yuan, Zhiqiang Li, Yuegen Liu Wei Wang Chaoping Xie, Xuming Wen, and Qien Yu. 2022. UPST-NeRF: Universal Photorealistic Style Transfer of Neural Radiance Fields for 3D Scene. *arXiv preprint arXiv:2208.07059* (2022).

Pei-Ze Chiang, Meng-Shiun Tsai, Hung-Yi Tseng, Wei-Sheng Lai, and Wei-Chen Chiu. 2022. Styling 3d scene via implicit representation and hypernetwork. In *Proceedings of the IEEE/CVF Winter Conference on Applications of Computer Vision*. 1475–1484.

Karan Desai and Justin Johnson. 2021. VirTex: Learning Visual Representations From Textual Annotations. In *Proceedings of the IEEE/CVF Conference on Computer Vision and Pattern Recognition (CVPR)*. 11162–11173.

Terrance DeVries, Miguel Angel Bautista, Nitish Srivastava, Graham W. Taylor, and Joshua M. Susskind. 2021. Unconstrained Scene Generation With Locally Conditioned Radiance Fields. In *Proceedings of the IEEE/CVF International Conference on Computer Vision (ICCV)*. 14304–14313.

Emilien Dupont, Adam Goliński, Milad Alizadeh, Yee Whye Teh, and Arnaud Doucet. 2021. Coin: Compression with implicit neural representations. *arXiv preprint arXiv:2103.03123* (2021).

Zhiwen Fan, Yifan Jiang, Peihao Wang, Xinyu Gong, Dejia Xu, and Zhangyang Wang. 2022. Unified implicit neural stylization. In *Computer Vision–ECCV 2022: 17th European Conference, Tel Aviv, Israel, October 23–27, 2022, Proceedings, Part XV*. 636–654.

Rinon Gal, Or Patashnik, Haggai Maron, Gal Chechik, and Daniel Cohen-Or. 2021. Stylegan-nada: Clip-guided domain adaptation of image generators. *arXiv preprint arXiv:2108.00946* (2021).

Bingchen Gong, Yuehao Wang, Xiaoguang Han, and Qi Dou. 2023. RecolorNeRF: Layer Decomposed Radiance Fields for Efficient Color Editing of 3D Scenes. *arXiv preprint arXiv:2301.07958* (2023).

Ian Goodfellow, Jean Pouget-Abadie, Mehdi Mirza, Bing Xu, David Warde-Farley, Sherjil Ozair, Aaron Courville, and Yoshua Bengio. 2014. Generative Adversarial Nets. In *Advances in Neural Information Processing Systems*, Vol. 27.

Jiatao Gu, Lingjie Liu, Peng Wang, and Christian Theobalt. 2022. StyleNeRF: A Style-based 3D Aware Generator for High-resolution Image Synthesis. In *Advances in Neural Information Processing Systems*.

Ishaan Gulrajani, Faruk Ahmed, Martin Arjovsky, Vincent Dumoulin, and Aaron C Courville. 2017. Improved Training of Wasserstein GANs. In *Advances in Neural Information Processing Systems*, Vol. 30.

Ayaan Haque, Matthew Tancik, Alexei A Efros, Aleksander Holynski, and Angjoo Kanazawa. 2023. Instruct-NeRF2NeRF: Editing 3D Scenes with Instructions. *arXiv preprint arXiv:2303.12789* (2023).

Jonathan Ho, Ajay Jain, and Pieter Abbeel. 2020a. Denoising diffusion probabilistic models. *Advances in Neural Information Processing Systems* 33 (2020). 6840–6851.

Jonathan Ho, Ajay Jain, and Pieter Abbeel. 2020b. Denoising Diffusion Probabilistic Models. In *Advances in Neural Information Processing Systems*, H. Larochelle, M. Ranzato, R. Hadsell, M.F. Balcan, and H. Lin (Eds.), Vol. 33. 6840–6851.

Yi-Hua Huang, Yue He, Yu-Jie Yuan, Yu-Kun Lai, and Lin Gao. 2022. Stylizednerf: consistent 3d scene stylization as stylized nerf via 2d-3d mutual learning. In *Proceedings of the IEEE/CVF Conference on Computer Vision and Pattern Recognition*. 18342–18352.

Ajay Jain, Ben Mildenhall, Jonathan T. Barron, Pieter Abbeel, and Ben Poole. 2022. Zero-Shot Text-Guided Object Generation with Dream Fields. (2022).

Chiyu Jiang, Avneesh Sud, Ameesh Makadia, Jingwei Huang, Matthias Nießner, Thomas Funkhouser, et al. 2020. Local implicit grid representations for 3d scenes. In *Proceedings of the IEEE/CVF Conference on Computer Vision and Pattern Recognition*. 6001–6010.

Sosuke Kobayashi, Eiichi Matsumoto, and Vincent Sitzmann. 2022. Decomposing NeRF for Editing via Feature Field Distillation. In *NeurIPS*.

Alex Krizhevsky, Ilya Sutskever, and Geoffrey E Hinton. 2017. Imagenet classification with deep convolutional neural networks. *Commun. ACM* 60, 6 (2017). 84–90.

Boyi Li, Kilian Q Weinberger, Serge Belongie, Vladlen Koltun, and René Ranftl. 2022b. Language-driven semantic segmentation. *arXiv preprint arXiv:2201.03546* (2022).

Junnan Li, Dongxu Li, Silvio Savarese, and Steven Hoi. 2023. BLIP-2: Bootstrapping Language-Image Pre-training with Frozen Image Encoders and Large Language Models. *arXiv:2301.12597 [cs.CV]*

Junnan Li, Dongxu Li, Caiming Xiong, and Steven Hoi. 2022a. BLIP: Bootstrapping Language-Image Pre-training for Unified Vision-Language Understanding and Generation. In *ICML*.

Chen-Hsuan Lin, Jun Gao, Luming Tang, Towaki Takikawa, Xiaohui Zeng, Xun Huang, Karsten Kreis, Sanja Fidler, Ming-Yu Liu, and Tsung-Yi Lin. 2023. Magic3D: High-Resolution Text-to-3D Content Creation. In *IEEE Conference on Computer Vision and Pattern Recognition (CVPR)*.

Tsung-Yi Lin, Michael Maire, Serge Belongie, James Hays, Pietro Perona, Deva Ramanan, Piotr Dollár, and C Lawrence Zitnick. 2014. Microsoft coco: Common objects in context. (2014), 740–755.

Steven Liu, Xiuming Zhang, Zhoutong Zhang, Richard Zhang, Jun-Yan Zhu, and Bryan Russell. 2021. Editing Conditional Radiance Fields. In *Proceedings of the International Conference on Computer Vision (ICCV)*.

Xian Liu, Yinghao Xu, Qianyi Wu, Hang Zhou, Wayne Wu, and Bolei Zhou. 2022. Semantic-aware implicit neural audio-driven video portrait generation. In *Computer Vision–ECCV 2022: 17th European Conference, Tel Aviv, Israel, October 23–27, 2022, Proceedings, Part XXXVII*. Springer, 106–125.

Nelson Max. 1995. Optical models for direct volume rendering. *IEEE Transactions on Visualization and Computer Graphics* 1, 2 (1995), 99–108.

Lars Mescheder, Michael Oechsle, Michael Niemeyer, Sebastian Nowozin, and Andreas Geiger. 2019. Occupancy networks: Learning 3d reconstruction in function space. In *Proceedings of the IEEE/CVF conference on computer vision and pattern recognition*. 4460–4470.

Gal Metzer, Elad Richardson, Or Patashnik, Raja Giryes, and Daniel Cohen-Or. 2022. Latent-NeRF for Shape-Guided Generation of 3D Shapes and Textures. *arXiv preprint arXiv:2211.07600* (2022).

Aryan Mikaeili, Or Perel, Daniel Cohen-Or, and Ali Mahdavi-Amiri. 2023. SKED: Sketch-guided Text-based 3D Editing. *arXiv preprint arXiv:2303.10735* (2023).

Ben Mildenhall, Pratul P. Srinivasan, Matthew Tancik, Jonathan T. Barron, Ravi Ramamoorthi, and Ren Ng. 2020. NeRF: Representing Scenes as Neural Radiance Fields for View Synthesis. In *Proceedings of the European Conference on Computer Vision (ECCV)*.

Ben Mildenhall, Pratul P. Srinivasan, Rodrigo Ortíz-Cayón, Nima Khademi Kalantari, Ravi Ramamoorthi, Ren Ng, and Abhishek Kar. 2019. Local Light Field Fusion: Practical View Synthesis with Prescriptive Sampling Guidelines. *ACM Transactions on Graphics (TOG)* (2019).

Alexander Mordvintsev, Nicola Pezzotti, Ludwig Schubert, and Chris Olah. 2018. Differentiable image parameterizations. *Distill* 3, 7 (2018), e12.

Alex Nichol, Prafulla Dhariwal, Aditya Ramesh, Pranav Shyam, Pamela Mishkin, Bob McGrew, Ilya Sutskever, and Mark Chen. 2021. GLIDE: Towards Photorealistic Image Generation and Editing with Text-Guided Diffusion Models. In *International Conference on Machine Learning*.

Michael Niemeyer and Andreas Geiger. 2021a. CAMPARI: Camera-Aware Decomposed Generative Neural Radiance Fields. In *Proc. of the International Conf. on 3D Vision (3DV)*.

Michael Niemeyer and Andreas Geiger. 2021b. GIRAFFE: Representing Scenes As Compositional Generative Neural Feature Fields. In *Proceedings of the IEEE/CVF Conference on Computer Vision and Pattern Recognition (CVPR)*. 11453–11464.

Dong Huk Park, Samaneh Azadi, Xihui Liu, Trevor Darrell, and Anna Rohrbach. 2021. Benchmark for compositional text-to-image synthesis. (2021).

Jeong Joon Park, Peter Florence, Julian Straub, Richard Newcombe, and Steven Lovegrove. 2019. DeepSDF: Learning continuous signed distance functions for shape representation. In *Proceedings of the IEEE/CVF conference on computer vision and pattern recognition*. 165–174.

Ben Poole, Ajay Jain, Jonathan T. Barron, and Ben Mildenhall. 2023. DreamFusion: Text-to-3D using 2D Diffusion. In *The Eleventh International Conference on Learning Representations*.

Alec Radford, Jong Wook Kim, Chris Hallacy, Aditya Ramesh, Gabriel Goh, Sandhini Agarwal, Girish Sastry, Amanda Askell, Pamela Mishkin, Jack Clark, Gretchen Krueger, and Ilya Sutskever. 2021. Learning Transferable Visual Models From Natural Language Supervision. In *Proceedings of the 38th International Conference on Machine Learning*.

Nasim Rahaman, Aristide Baratin, Devansh Arpit, Felix Draxler, Min Lin, Fred A. Hamprecht, Yoshua Bengio, and Aaron Courville. 2019. On the Spectral Bias of Neural Networks. In *Proceedings of the 36th International Conference on Machine Learning*.

Aditya Ramesh, Prafulla Dhariwal, Alex Nichol, Casey Chu, and Mark Chen. 2022. Hierarchical Text-Conditional Image Generation with CLIP Latents. *ArXiv* abs/2204.06125 (2022).

Robin Rombach, Andreas Blattmann, Dominik Lorenz, Patrick Esser, and Björn Ommer. 2022. High-Resolution Image Synthesis With Latent Diffusion Models. In *Proceedings of the IEEE/CVF Conference on Computer Vision and Pattern Recognition (CVPR)*. 10684–10695.

Chitwan Saharia, William Chan, Saurabh Saxena, Lala Li, Jay Whang, Emily Denton, Seyed Kamyar Seyed Ghasemipour, Raphael Gontijo-Lopes, Burcu Karagol Ayan, Tim Salimans, Jonathan Ho, David J. Fleet, and Mohammad Norouzi. 2022. Photo-realistic Text-to-Image Diffusion Models with Deep Language Understanding. In *Advances in Neural Information Processing Systems*.

Katja Schwarz, Yiyi Liao, Michael Niemeyer, and Andreas Geiger. 2020. GRAF: Generative Radiance Fields for 3D-Aware Image Synthesis. In *Advances in Neural Information Processing Systems*, Vol. 33. 20154–20166.

Vincent Sitzmann, Eric R. Chan, Richard Tucker, Noah Snavely, and Gordon Wetzstein. 2020a. MetaSDF: Meta-Learning Signed Distance Functions. In *arXiv*.

Vincent Sitzmann, Julien N.P. Martel, Alexander W. Bergman, David B. Lindell, and Gordon Wetzstein. 2020b. Implicit Neural Representations with Periodic Activation Functions. In *Proc. NeurIPS*.

Vincent Sitzmann, Michael Zollhöfer, and Gordon Wetzstein. 2019. Scene Representation Networks: Continuous 3D-Structure-Aware Neural Scene Representations. In *Advances in Neural Information Processing Systems*.

Jiaming Song, Chenlin Meng, and Stefano Ermon. 2021. Denoising Diffusion Implicit Models. In *International Conference on Learning Representations*.

Yang Song and Stefano Ermon. 2020. Improved Techniques for Training Score-Based Generative Models. In *Advances in Neural Information Processing Systems*, Vol. 33. 12438–12448.

Yannick Strümpler, Janis Postels, Ren Yang, Luc Van Gool, and Federico Tombari. 2022. Implicit neural representations for image compression. In *Computer Vision–ECCV 2022: 17th European Conference, Tel Aviv, Israel, October 23–27, 2022, Proceedings, Part XXVI*. Springer, 74–91.

Kun Su, Mingfei Chen, and Eli Shlizerman. 2022. INRAS: Implicit Neural Representation for Audio Scenes. 35 (2022), 8144–8158. https://proceedings.neurips.cc/paper_files/paper/2022/file/35d5ad984cc0ddd84c6f1c177a2066e5-Paper-Conference.pdf

Filip Szatkowski, Karol J Piczak, Przemysław Spurek, Jacek Tabor, and Tomasz Trzeiński. 2022. HyperSound: Generating Implicit Neural Representations of Audio Signals with Hypernetworks. *arXiv preprint arXiv:2211.01839* (2022).

Matthew Tancik, Pratul Srinivasan, Ben Mildenhall, Sara Fridovich-Keil, Nithin Raghavan, Utkarsh Singhal, Ravi Ramamoorthi, Jonathan Barron, and Ren Ng. 2020. Fourier Features Let Networks Learn High Frequency Functions in Low Dimensional Domains. In *Advances in Neural Information Processing Systems*, Vol. 33.

Can Wang, Menglei Chai, Mingming He, Dongdong Chen, and Jing Liao. 2022a. CLIP-NeRF: Text-and-Image Driven Manipulation of Neural Radiance Fields. In *IEEE/CVF Conference on Computer Vision and Pattern Recognition, CVPR 2022, New Orleans, LA, USA, June 18–24, 2022*.

Haochen Wang, Xiaodan Du, Jiahao Li, Raymond A. Yeh, and Greg Shakhnarovich. 2022b. Score Jacobian Chaining: Lifting Pretrained 2D Diffusion Models for 3D Generation. *CoRR* abs/2212.00774 (2022).

Qiling Wu, Jianchao Tan, and Kun Xu. 2022. PaletteNeRF: Palette-based Color Editing for NeRFs. *arXiv preprint arXiv:2212.12871* (2022).

Yu-Jie Yuan, Yang-Tian Sun, Yu-Kun Lai, Yuewen Ma, Rongfei Jia, and Lin Gao. 2022. NeRF-editing: geometry editing of neural radiance fields. In *Proceedings of the IEEE/CVF Conference on Computer Vision and Pattern Recognition*. 18353–18364.

Xiaohua Zhai, Xiao Wang, Basil Mustafa, Andreas Steiner, Daniel Keysers, Alexander Kolesnikov, and Lucas Beyer. 2022. LiT: Zero-Shot Transfer With Locked-Image Text Tuning. In *Proceedings of the IEEE/CVF Conference on Computer Vision and Pattern Recognition (CVPR)*. 18123–18133.

Richard Zhang, Phillip Isola, Alexei A Efros, Eli Shechtman, and Oliver Wang. 2018. The unreasonable effectiveness of deep features as a perceptual metric. (2018), 586–595.

Peng Zhou, Lingxi Xie, Bingbing Ni, and Qi Tian. 2021. CIPS-3D: A 3D-Aware Generator of GANs Based on Conditionally-Independent Pixel Synthesis. *arXiv:2110.09788 [cs.CV]*

A IMPLEMENTATION DETAILS

In this section we provide additional implementation details.

A.1 Pose Sampling

In each training step, we sample a camera pose from a range of distances and angles, depending on the scene type. In the blender and 360 scenes, we sample azimuth and elevation angles in the ranges: $\theta \in [-180^\circ, 180^\circ]$, $\phi \in [-90^\circ, 15^\circ]$. For the radius, we first calculate the initial distance according to eq. (10) and then randomly sample the radius around this value. In llff dataset [Mildenhall et al. 2019] we sample the camera pose from a spiral curve as used in the original NeRF implementation². The curve is randomly sampled from a range of distances and radii in each axis. After sampling a camera pose, we recenter its rays around the ROI by moving its center location according to the center of mass inside the ROI (tracked by exponential moving average during training), but allow with a probability $p \in [0, 1]$ (hyperparameter, set to 0.1 in our experiments) to recenter the rays to a different point inside the ROI, with the aim of obtaining more versatile objects and densities. Additionally, we set the near and far planes (n, f) according to the box location and size in order to be more concentrated around the ROI and get more sample points per ray in this area:

$$n = d - \frac{D}{2}, \quad f = d + D, \quad (14)$$

where d is the distance of the camera from the center of mass inside the box and D is the box diagonal length.

A.2 Hyperparameters

In our experiments we set the max transmittance of L_T , the max variance of L_D and the weights of the losses to: $\tau = 0.88$, $\rho = 0.2$, $\lambda_T = 0.25$, $\lambda_D = 4$. We use the same network architecture as in [Mildenhall et al. 2020] and the same hyperparameters and learning rates. To guide our model, we use the CLIP B/32 architecture.

A.3 Training

We train our model with a random seed value of 123 for all of our experiments. In experiments, we render the views at 168x168 resolution and up-sample to 224x224 resolution before feeding them to CLIP [Radford et al. 2021]. In the Comparisons and a Ablation study sections, we train the generator for 40,000 iterations and for the other figures in the main paper, the views resolution and the number of iterations depends on the complexity of the synthesized object and hardware limitations. We train with 4×24 GB A5000 GPUs. Training takes between a few hours to one day depending on the scene, object complexity, view resolution and number of iterations.

A.4 Directional Dependent prompts

As described in the main paper, each iteration we concatenate a text prompt to the input caption depending on the camera location in the scene. We use the direction prompts below depending on the location:

- ", top-down view"

²<https://github.com/bmild/nerf>

- ", front view"
- ", side view"
- ", back view"

In forward-facing scenes like llff dataset [Mildenhall et al. 2019] we use the first three captions.

B ADDITIONAL EXPERIMENTS DETAILS

In this section we provide additional information regarding the experiments from the main paper.

B.1 Metrics

In our quantitative evaluation we report four metrics: CLIP Direction Similarity, CLIP Direction Consistency, LPIPS and R-Precision.

CLIP Direction Similarity introduced in [Gal et al. 2021] as a direction loss which measures the similarity between the change in the text descriptions and the change in the images. We use a variation of this metric so that high similarity will have high metric score:

$$\begin{aligned} \Delta T &= E_T(T_e) - E_T(T_o) \\ \Delta I &= E_I(I_e) - E_I(I_o) \\ L_{direction} &= \frac{\Delta T \cdot \Delta I}{|\Delta T| |\Delta I|} \end{aligned} \quad (15)$$

When E_T, E_I are the text and image encoders of CLIP, T_e, T_o are the text captions describing the edited and original scene inside the ROI and I_e, I_o are the according edited and original scenes views. In our experiments on the fern llff scene [Mildenhall et al. 2019], we set T_o to: "a photo of a fern trunk".

CLIP Direction Score introduced in [Haque et al. 2023] measures the consistency between adjacent frames by calculating the CLIP embeddings of two corresponding pairs of consecutive views, one from the original scene and one from the edited scene. Similar to CLIP Direction Similarity metric, we then compute the similarity between the change in the original and edited scene views to get the final consistency score:

$$\begin{aligned} \Delta I_o &= E_I(I_{i+1}^o) - E_I(I_i^o) \\ \Delta I_e &= E_I(I_{i+1}^e) - E_I(I_i^e) \\ L_{direction} &= \frac{\Delta I_o \cdot \Delta I_e}{|\Delta I_o| |\Delta I_e|} \end{aligned} \quad (16)$$

When I_i^o, I_{i+1}^o and I_i^e, I_{i+1}^e are the original and edited consecutive views pairs. In our experiments we compute this score on six consecutive views and average the results.

LPIPS or Learned Perceptual Image Patch Similarity, is used to judge the perceptual similarity between two images, [Zhang et al. 2018] shows that this metric match human perception. The metric computes the similarity between the activation's of the two images for some network architecture. In our experiments we use LPIPS with pre-trained alexnet architecture [Krizhevsky et al. 2017] to measure the background similarity between the original and the

edited scenes by masking the ROI region.

R-Precision [Park et al. 2021] measures how well a rendered view of the synthesis object align with the text caption used to generate it. It computes the precision of the rendered views over a group of text captions using a retrieval model. Similar to DreamFields [Jain et al. 2022] we collect an object-centric captions dataset from COCO dataset [Lin et al. 2014] and sample 20 captions that will be used for training our model. We then compute the precision of the rendered views per synthesis object over the 153 captions. As the language image model backbone of the score, we use both CLIP [Radford et al. 2021] and BLIP2 [Li et al. 2023], since we use CLIP to train our model.

C CONCURRENT WORK

Concurrently with our work, Instruct-NeRF2NeRF [Haque et al. 2023] present a diffusion-based method for editing a NeRF scene guided by text instructions. It utilizes InstructPix2Pix [Brooks et al. 2022], which enables editing images based on text instructions. The edit is preformed by iteratively updating the image dataset of the original scene while training NeRF using these edited images. They demonstrate an impressive high quality local edit results on real scenes but sometimes can't preserve the rest of the scene and get a blurrier scene compared to the original, and sometimes even introduce texture and color changes to the entire scene.

SKED [Mikaeili et al. 2023] research the possibility to edit a NeRF scene using guidance from 2D sketches from different views additional to an input text prompt describing the edit. They utilize the SDS loss presented in [Poole et al. 2023] to steer the edit towards the input caption and present preservation and silhouette priors to preserve the original scene and to preform the edit only on the sketched regions. In experiments they apply their method mainly on synthetic objects and demonstrate its applicability on objects insertion and replacement tasks such as hats, flowers and glasses.

In SINE [Bao et al. 2023], they suggest a method for editing NeRF scene by only editing a single view, and than apply the edit to the entire scene. To do this they encode the changes in geometry and texture over the original NeRF scene, by learning a prior-guided editing field. Using this field they render the modified object geometry and color and present color compositing layer supervised by the single edited view to apply the edit on novel views. They apply their method on real and synthetic scenes by changing the geometry and texture of objects in the scene.

D ADDITIONAL EXAMPLES

We provide additional examples for the applications in the main paper. In Figure 11 we show another example for object replacement and in Figure 12 we preform the texture conversion task on a different 360 scene.

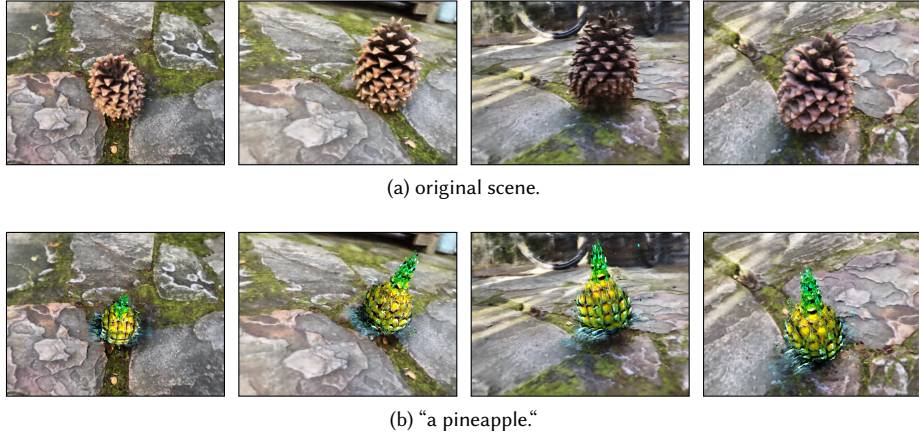


Fig. 11. **Object replacement in 360 pinecone scene.** We replace the original pinecone object with pineapple using our proposed object replacement method.



Fig. 12. **Texture conversion on 360 vasedeck scene.** Using the same method as in Figure 8 in the main paper.